

EVOLUTION OF GALAXY STELLAR MASS FUNCTIONS, MASS DENSITIES, AND MASS TO LIGHT RATIOS FROM $Z \sim 7$ TO $Z \sim 4$

VALENTINO GONZÁLEZ¹, IVO LABBÉ^{2,3}, RYCHARD J. BOUWENS¹, GARTH ILLINGWORTH¹, MARIJN FRANX⁴, MARISKA KRIEK⁵

Draft version November 13, 2018

ABSTRACT

We derive stellar masses from SED fitting to rest-frame optical and UV fluxes for 401 star-forming galaxies at $z \sim 4, 5,$ and 6 from Hubble-WFC3/IR observations of the ERS combined with the deep GOODS-S Spitzer/IRAC data (and include a previously-published $z \sim 7$ sample). A mass-luminosity relation with strongly luminosity-dependent \mathcal{M}/L_{UV} ratios is found for the largest sample (299 galaxies) at $z \sim 4$. The relation $\mathcal{M} \propto L_{UV,1500}^{1.7(\pm 0.2)}$ has a well-determined intrinsic sample variance of 0.5 dex. This relation is also consistent with the more limited samples at $z \sim 5 - 7$. This $z \sim 4$ mass-luminosity relation, and the well-established faint UV luminosity functions at $z \sim 4 - 7$, are used to derive galaxy mass functions (MF) to masses $\mathcal{M} \sim 10^8$ at $z \sim 4 - 7$. A bootstrap approach is used to derive the MFs to account for the large scatter in the \mathcal{M} - L_{UV} relation and the luminosity function uncertainties, along with an analytical crosscheck. The MFs are also corrected for the effects of incompleteness. The incompleteness-corrected MFs are steeper than previously found, with slopes $\alpha_M \sim -1.4$ to -1.6 at low masses. These slopes are, however, still substantially flatter than the MFs obtained from recent hydrodynamical simulations. We use these MFs to estimate the stellar mass density (SMD) of the universe to a fixed $M_{UV,AB} < -18$ as a function of redshift and find a SMD growth $\propto (1+z)^{-3.4 \pm 0.8}$ from $z \sim 7$ to $z \sim 4$. We also derive the SMD from the completeness-corrected MFs to a mass limit $\mathcal{M} \sim 10^8 M_\odot$. Such completeness-corrected MFs and the derived SMDs will be particularly important for model comparisons as future MFs reach to lower masses.

Subject headings: galaxies: evolution — galaxies: high-redshift

1. INTRODUCTION

Measurements of the stellar mass of high-redshift galaxies ($z \gtrsim 4$) provide important constraints on scenarios of galaxy formation and early evolution. For example, the evidence for a strong correlation between the observed star formation rate (SFR) and stellar mass (Stark et al. 2009; Labbé et al. 2010a,b), with little apparent evolution between $z \sim 3$ and $z \sim 7$ (Stark et al. 2009; González et al. 2010), suggests an epoch of exponential growth which, interestingly, is similar to that found in simulations (e.g. Finlator et al. 2010).

Recent deep near-IR WFC3/IR observations over the ERS field (Windhorst et al. 2010) combined with pre-existing deep GOODS IRAC data provide access to the rest-frame UV and optical wavelengths of $4 < z < 7$ star forming galaxies and hence reasonably accurate estimates of their \mathcal{M}/L ratios and stellar masses. The substantial samples of $z > 4$ galaxies detected with WFC3/IR span a range in stellar mass, allowing the derivation of mass functions (MFs).

MFs are fundamental characteristics of the galaxy population but in practice, they are difficult to compute directly, especially at high redshift because of selection ef-

fects, incompleteness, and contamination by interlopers. An alternative approach to derive the MF is to start with the well-determined UV LF at these redshifts and convert to stellar mass using an average \mathcal{M}/L (e.g. McLure et al. 2009). The main advantage is that LFs are corrected for all selection effects in the data and reach very faint limits, although such a simple approach does not take into account any possible luminosity dependence or scatter of the \mathcal{M}/L . In this Letter, we estimate improved MFs at $4 < z < 7$ from the published UV-LFs by deriving a relation between UV luminosity and stellar masses. We also estimate the scatter in the \mathcal{M}/L , which allows us to correct for incompleteness at low stellar masses. We use the MFs to compute the stellar mass density (SMD) of the universe at $z = 4, 5, 6$ and 7 .

We adopt an $\Omega_M = 0.3, \Omega_\Lambda = 0.7$ cosmology with $H_0 = 70 \text{ km s}^{-1} \text{ Mpc}^{-1}$ throughout. All magnitudes are in the AB system (Oke & Gunn 1983).

2. GALAXY SAMPLE FROM HST AND SPITZER DATA

The sources used here for determinations of the \mathcal{M}/L ratios and $z = 4 - 6$ MFs were found in the recent Hubble-WFC3/IR observations of the ERS field. Both the GOODS ACS optical ($B_{435}V_{606}i_{775}z_{850}$) and the WFC3/IR ($Y_{098}J_{110}H_{160}$) data reach depths of ~ 28 mag ($5\sigma, 0.35''$ -diameter apertures, see Bouwens et al. 2010; Giavalisco et al. 2004). All sources have Spitzer/IRAC coverage with depths of 27.8 and 27.1 in the [3.6] and [4.5] channels, respectively (1σ in $2.4''$ apertures). The $z \sim 7$ sample is taken from (Labbé et al. 2010a).

The $z \sim 4, 5, 6$ sample totals 679 objects, consisting of 524 B , 123 V , and 32 i -dropouts that were selected with

¹ Astronomy Department, University of California, Santa Cruz, CA 95064

² Carnegie Observatories, 813 Santa Barbara Street, Pasadena, CA 91101

³ Hubble Fellow

⁴ Leiden Observatory, Leiden University, NL-2300 RA Leiden, Netherlands

⁵ Department of Astrophysical Sciences, Princeton University, Princeton, NJ 08544

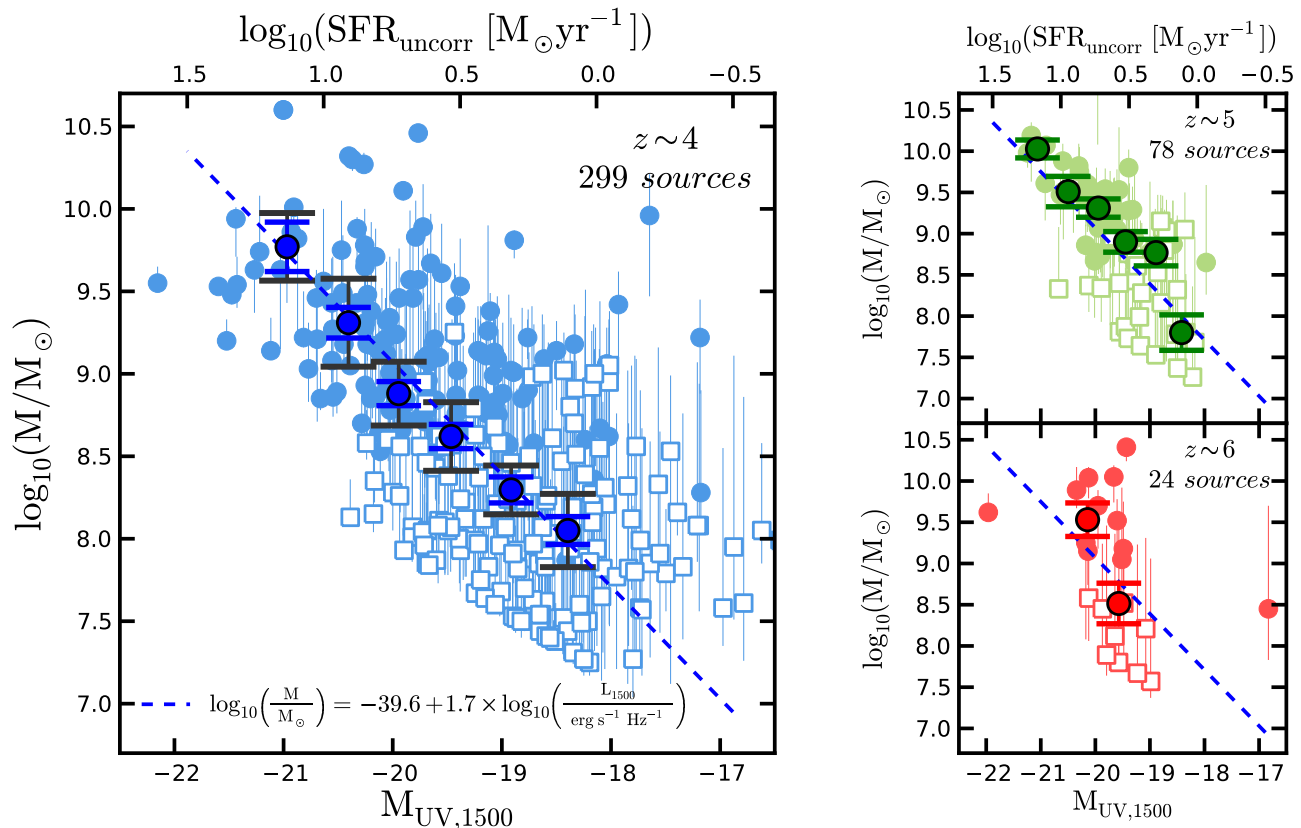


FIG. 1.— Stellar masses as a function of UV Luminosity ($M_{UV,1500} = 51.63 - 2.5 \times \log_{10}(L_{UV,1500}[\text{erg s}^{-1} \text{Hz}^{-1}])$) for the $z \sim 4, 5$, and 6 samples. $\text{SFR}_{\text{uncorr}}$ (top axis) is derived using the Madau et al. (1998) conversion formula (no extinction correction). The final sample of 401 sources with FAST SED-fit mass estimates is shown here. Open squares indicate low-S/N measurements ($< 2\sigma$ in [3.6]). The darker symbols in each panel represent the median mass of the sample ($\sim 0.5 M_{UV,1500}$ -mag bins). The small error bars represent the bootstrapped errors. The larger black error bars include a conservative estimate of the systematics computed by comparing the estimated median mass at a given luminosity with the mass estimated from the stacked SEDs at the same luminosity. The dashed blue line (slope = 1.7 ± 0.2) represents the mean trend between $\log_{10}M$ and $M_{UV,1500}$ at $z \sim 4$. It is consistent with no evolution with redshift. The scatter at the luminous end (± 0.5 dex), where photometric errors are small, is intrinsic (see Figure 2).

the same criteria as Bouwens et al. (2007):

$z \sim 4$ *B*-dropouts:

$$(B_{435} - V_{606} > 1.1) \wedge [B_{435} - V_{606} > (V_{606} - z_{850}) + 1.1] \\ \wedge (V_{606} - z_{850} < 1.6)$$

$z \sim 5$ *V*-dropouts:

$$\{[V_{606} - i_{775} > 0.9(i_{775} - z_{850})] \vee (V_{606} - i_{775} > 2)\} \\ \wedge (V_{606} - i_{775} > 1.2) \wedge (i_{775} - z_{850} < 1.3)$$

$z \sim 6$ *i*-dropouts⁶:

$$(i_{775} - z_{850} > 1.3) \wedge (z_{850} - J_{125} < 0.8)$$

The rest-frame optical photometry from Spitzer/IRAC is ideally suited for deriving stellar masses at these redshifts (e.g. Papovich et al. 2001; Yan et al. 2005; Labbé et al. 2010a). A challenge is that the broad IRAC PSF usually results in these faint sources being contaminated by foreground neighbors. To obtain

reliable IRAC fluxes we use the deblending method of Labbé et al. (2006, see also González et al. 2010; Labbé et al. 2010b,a; Wuyts et al. 2007; de Santis et al. 2007). Briefly, this method uses the higher-resolution HST images to create models of both the foreground neighbors and the source itself. We convolve each model image with a kernel to simulate the IRAC observations. We fit for all the sources simultaneously (with independent normalization factors) and subtract the best fits for the neighbors. In the clean image of each dropout we are able to perform standard aperture photometry. We use $2.5''$ -diameter apertures and correct the fluxes to total assuming stellar profiles ($1.8\times$ in both channels).

As expected, our cleaning procedure does not work for every source. We restrict our sample to the 60% of sources with the best χ^2 residuals. This reduces the number of non-optimal subtractions to $< 8\%$. The final sample suitable for deriving masses from the HST+Spitzer data totals 401 sources: 299 $z \sim 4$, 78 $z \sim 5$, and 24 at $z \sim 6$. We do not expect this selection step to introduce any important biases, since it depends on the distribution of the non-associated neighbors of the source. Of the

⁶ Slightly modified, Bouwens et al. 2010, in prep.

remaining sources, $\sim 50\%$ have low IRAC S/N ($< 2\sigma$ in [3.6]).

3. STELLAR MASS ESTIMATES FROM SED FITS

We use the FAST SED-fitting code (Kriek et al. 2009) to derive stellar masses of the 401 $z \sim 4-6$ sources from SED fits with the full suite of fitted parameters. For all sources we fit the broadband ACS+WFC3/IR+IRAC [3.6] and [4.5] fluxes using the Bruzual & Charlot (2003, BC03) models with a Salpeter (1955) initial mass function (IMF, 0.1–100 M_{\odot}) and assuming a 0.2 Z_{\odot} metallicity. We also include the sample of $z \sim 7$ galaxies with similarly-determined masses from Labbé et al. (2010a).

The SFH cannot be uniquely determined from broadband SEDs due to well-known degeneracies between the star formation timescale, age, and dust extinction. We have assumed a SFH with a constant SFR. Different SFHs introduce systematic offsets to the mass determinations, largely independent of redshift (cf. Papovich et al. 2010). The systematic differences between masses based on declining, constant, or rising SFHs are typically $\lesssim 0.3$ dex (Finlator et al. 2007).

Figure 1 (left) shows the FAST SED-fit stellar masses (from HST+Spitzer data) versus UV luminosity (bottom axis). While the scatter is large (RMS ~ 0.5 dex), there is a clear trend of increasing mass with increasing UV luminosity. The stellar mass \mathcal{M} – $M_{UV,1500}$ relation at $z \sim 4$ is well-fit by $\log_{10}(\mathcal{M}) \propto 1.7(\pm 0.2)\log_{10}(L_{1500})$. The lower bound that appears at masses $< 10^8 M_{\odot}$ corresponds to the \mathcal{M}/L of the youngest model we allow (10 Myrs). This is a reasonable assumption for the majority of the sample, as IRAC detections in the stacks suggest that continuum is dominant, not emission lines. This is also not critical, since our inferred \mathcal{M}/L trend is insensitive to the cutoff. The $z \sim 4$ relation is consistent with the $z \sim 5$ sample, and, in zero-point, with the small $z \sim 6$ sample, and also with the $z \sim 7$ sample presented in (Labbé et al. 2010a).

Figure 2 explores the $z \sim 4$ \mathcal{M}/L ratio trend in more detail, showing that $\mathcal{M}/L_{UV,1500}$ depends on luminosity; the \mathcal{M}/L ratio is $\sim 5\times$ lower at $M_{UV,1500} = -18$ than at $M_{UV,1500} = -21$. This suggests that UV-faint galaxies contribute less to the global SMD than assumed in previous studies (Labbé et al. 2010b,a). However, due to the steep faint-end slope of the UV LF (e.g. Bouwens et al. 2010), their high number density makes their total contribution quite significant.

A striking aspect of the relation is the large scatter in \mathcal{M}/L . The observed sample variance (one standard deviation) for our sample is ~ 0.5 dex for $-21 < M_{UV,1500} < -18$. At the bright end $M_{UV,1500} < -20$ the scatter is largely intrinsic, whereas at the faint end $M_{UV,1500} > -19.5$ it is dominated by observational uncertainties. In particular, the stellar masses of sources with IRAC detections are much better constrained than IRAC-undetected sources. Photometric uncertainties contribute ~ 0.14 dex to the scatter at $M_{UV,1500} \sim -20$ (0.37 dex at -19). Moreover, we find that the \mathcal{M}/L ratio is tightly correlated with the $J - [3.6]$ color (standard deviation 0.18 dex, Figure 2, right), suggesting that the variation is real, and not an artifact of the modeling.

The relation in Figure 2 (right) also allows us to estimate the possible effect of contamination by emission lines (not included in our models). At $z \sim 4$, a 20% con-

tribution of H α to [3.6] would result in redder $J - [3.6]$ colors and hence overestimates of the \mathcal{M}/L and of the masses by 30%. This would affect the SMDs at all redshifts because they all rely on our $z \sim 4$ \mathcal{M}/L ratio estimates (see §4).

4. STELLAR MASS FUNCTIONS AT $Z \sim 4, 5, 6,$ AND 7.

The stellar MFs at a given redshift can be estimated by combining the LF at that redshift with an appropriate \mathcal{M}/L relation. Since UV LFs have been derived from large samples to very faint limits and carefully corrected for a wide range of potential biases, they constitute an excellent basis for determining MFs. The calibration of $\log(\mathcal{M})$ vs $M_{UV,1500}$ in Figures 1 and 2 provides the means to transform the $z \sim 4-7$ UV-LFs into MFs.

However, the scatter about the mean \mathcal{M} – $M_{UV,1500}$ relation is so large that ignoring it would produce significant errors. Galaxies with relatively low luminosity but high \mathcal{M}/L ratios, for example, contribute significantly at the high mass end of the MFs. Hence, we take care to determine the average \mathcal{M} – $M_{UV,1500}$ relation in a robust way, we characterize the scatter at the high mass end and use this estimate of the scatter at lower luminosities/masses where the observational uncertainties dominate.

We use two approaches to create the MFs. First, we use the individual points in Figure 1 as representative of the \mathcal{M} – $M_{UV,1500}$ distribution by bootstrap resampling them. To correct for incompleteness we add faint sources to the distribution. This important step increases the low mass slope of the MFs substantially. Second, we use the fitted \mathcal{M} – $M_{UV,1500}$ relation and an idealized model of its scatter to produce what we label as “analytic” versions of the MFs. We compare to other estimates as a cross-check.

Bootstrapped MFs: We start with the $z \sim 4-7$, UV-LFs of Bouwens et al. (2007, 2010) and draw 40000 luminosities from each LF in the range $-21.5 < M_{UV,1500} < -18$. We convert the luminosities to stellar masses by bootstrap re-sampling from the distribution of points at $z \sim 4$ in Figure 1. We use the $z \sim 4$ $\log(\mathcal{M}) - M_{UV,1500}$ distribution at all redshifts because it is well-defined over a wide range of luminosities and is consistent with the relations at other redshifts, including the $z \sim 7$ relation presented in Labbé et al. (2010a). To account for the uncertainties in the LFs we perturb their Schechter parametrizations within the uncertainties and repeat 5000 times. This “bootstrap” process results in the uncorrected MFs (Figure 3 open squares and error bars).

As a crosscheck we also derived a histogram MF at $z \sim 4$ directly from the masses of the $z \sim 4$ sample using the search volume for the B -dropouts. This straightforward process gives a MF that is identified in Figure 3 as the “direct MF” for comparison with the uncorrected “bootstrap MF”.

To correct the MFs for incompleteness at $\mathcal{M} < 10^{8.5} M_{\odot}$, we re-derive the MFs but now including fainter ($-18 < M_{UV,1500} < -15$) sources. We extrapolate the observed $\log(\mathcal{M})$ – $M_{UV,1500}$ relation to lower luminosities and assume that the low-luminosity scatter is similar to the scatter around $M_{UV,1500} \sim -18.5$. The resulting errors on the corrected points include an added uncertainty that is typically about 30–40%. This accounts for the LFs uncertainties (specially the faint end slope) and the

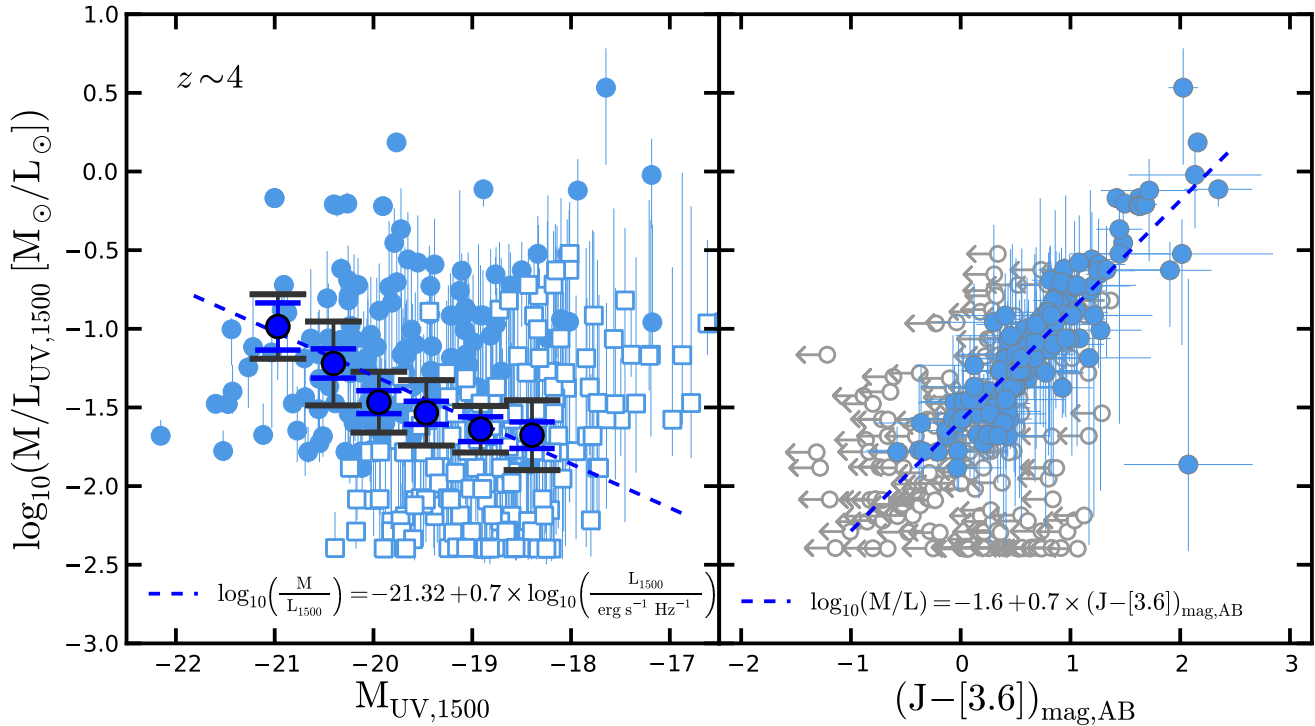


FIG. 2.— (left) \mathcal{M}/L ratio as a function of UV Luminosity for the $z \sim 4$ sample. Symbols and error bars as in Figure 1. The median \mathcal{M}/L ratio changes by a factor $5\times$ in the luminosity range our sample. (right) The correlation between the \mathcal{M}/L and $J - [3.6]$ color. Arrows indicate 2σ -upper limits. This tight relation suggests that the large scatter observed in the \mathcal{M}/L (left panel) is largely due to intrinsic variations in the UV-to-optical colors. Photometric scatter can only account for $\lesssim 0.14$ dex at $M_{UV,1500} \sim -20$ (0.37 dex at -19).

large scatter about the relations. Other sources of uncertainty may remain but further assessment is needed to fully evaluate them. Regardless, the current corrections must make these corrected MFs a better estimate of the true MFs. Applying the completeness corrections is a crucial step and significantly changes the slope of the MF at lower mass. The corrected MFs are shown in Figure 3 by the solid points and the solid color band, and are referred to as the *bootstrap* MFs.

Analytic MFs: The best fit \mathcal{M} - $M_{UV,1500}$ relation in Figure 1 at $z \sim 4$ is: $\mathcal{M} \propto L_{UV,1500}^{1.7(\pm 0.2)}$. We combine this relation with the same LFs as above to derive the *analytic* MFs (Figure 3). The large scatter needs to be accounted for in order to generate a realistic estimate. The mass distribution at a given luminosity is assumed to be log-normal with a standard deviation of 0.5 dex, centered on the fitted $\log(\mathcal{M})$ - $M_{UV,1500}$ relation. The resulting relation, normalized by the LF, is integrated over L to get the *analytic* MFs.

At lower masses, the slope of the MF is set by the faint-end slope of the UV-LFs and of the $\log(\mathcal{M})$ - $M_{UV,1500}$ relation. Extrapolating this \mathcal{M} - $M_{UV,1500}$ relation to lower luminosities results in steep low-mass slopes for the MFs of $-1.43(\pm 0.11)$, $-1.39(\pm 0.11)$, $-1.44(\pm 0.15)$, and $-1.55(\pm 0.21)$ at $z \sim 4, 5, 6,$ and 7 . These MF slopes are slightly flatter than the UV LF slopes ($\alpha = -1.7 - -2$; Bouwens et al. 2010). They are in good agreement with our completeness-corrected *bootstrap* MFs, and so provide a useful “sanity check” on those results. The standard deviation of 0.5 dex in the

$\log(\mathcal{M})$ - $M_{UV,1500}$ relation results in a slightly enhanced number density at the high-mass end compared to a case with no scatter. Our corrected MFs are considerably steeper than other MF determinations at high redshift (Stark et al. 2009) that do not apply completeness corrections. Truncating the analytic \mathcal{M} - $M_{UV,1500}$ relation at $M_{1500} < -18$ (to represent survey incompleteness) results in analytic MFs that are in good agreement with the non-corrected *bootstrap* MFs at low masses.

Comparisons to simulated MFs: The MFs derived here are substantially steeper at low masses than what has been found in the past at these redshifts. This is not unexpected given that it has not been typical to correct for incompleteness. While the corrections are uncertain in magnitude the sign of the correction is not. Interestingly, even with the corrected and steeper slopes, the observed MFs are quite different from what is seen in recent simulations (e.g. Choi & Nagamine 2010; Finlator et al. in preparation). The simulated MFs are steeper, with dramatically more low-mass sources than we find.

5. STELLAR MASS DENSITY AT $Z \sim 4, 5, 6,$ AND 7

The MFs can be integrated to determine the SMD of the universe at high redshift. First, we integrate the (uncorrected) *bootstrap* MFs to determine the SMD at $z = 4, 5, 6,$ and 7 to faint-luminosity limits ($M_{1500} < -18$ – Table 1; Figure 4 left). Fitting the SEDs using the observed fluxes rather than upper limits allows us to reach lower limits than those of Stark et al. (2009) at $z = 4 - 6$. To compare to those results, we correct their original $M_{1500} = -20$ limit to our

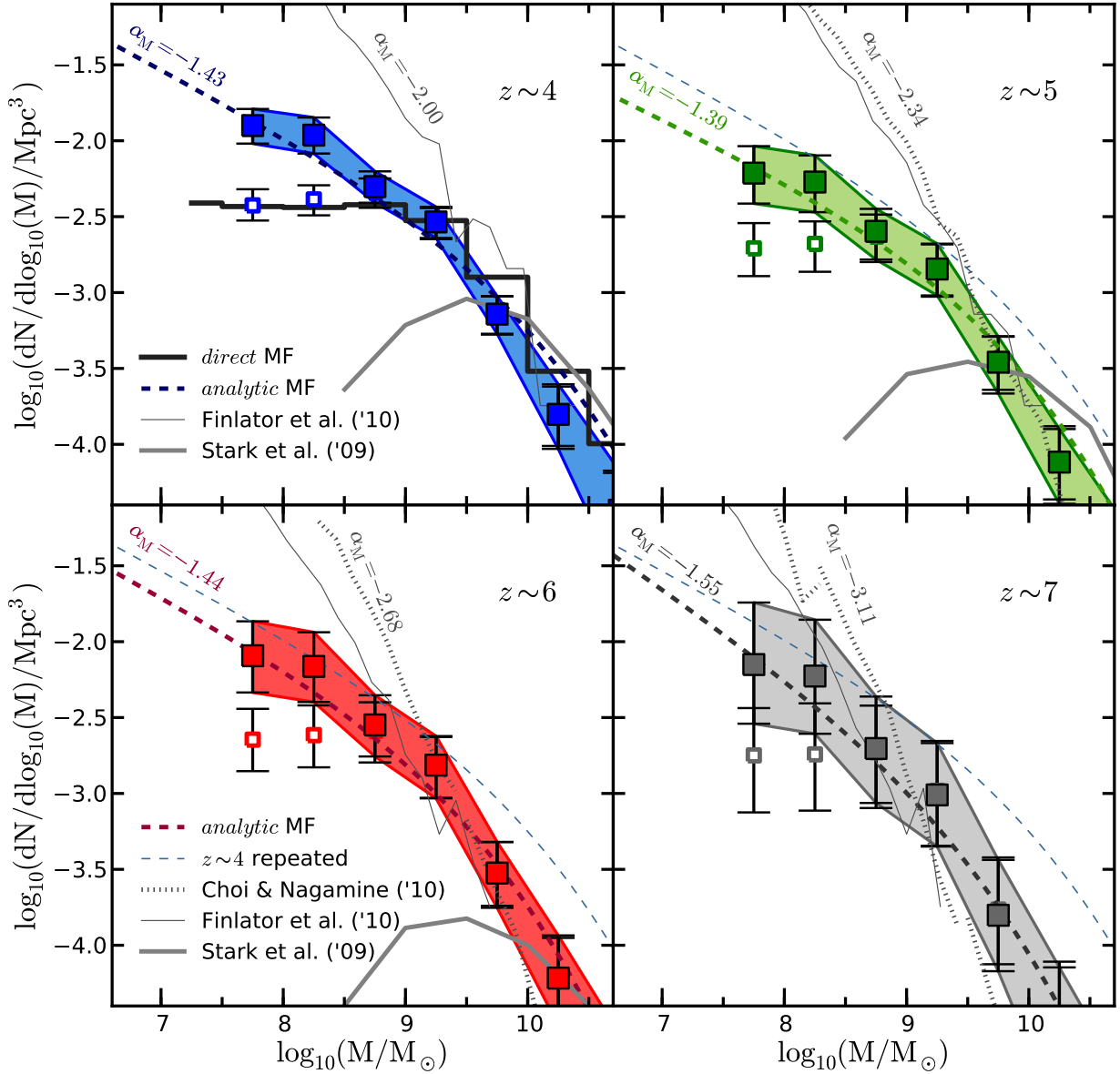


FIG. 3.— Stellar mass functions at $z \sim 4, 5, 6,$ and 7 derived from the $\log(\mathcal{M}) - M_{UV,1500}$ distribution for the $z \sim 4$ B -dropouts (Figure 1), and the Bouwens et al. (2007, 2010) UV-LFs at $z \sim 4 - 7$. The points are derived from the “bootstrap” approach (see text). Errors reflect uncertainties in the LF and the ~ 0.5 dex 1σ scatter of the $\mathcal{M} - M_{UV,1500}$ relation (Figure 1). Completeness-corrected values are estimated assuming that the $\mathcal{M} - M_{UV,1500}$ relation extends to fainter limits with similar scatter about the extrapolated mean trend ($M_{UV,1500} < -18$ uncorrected: open; corrected: filled; dark band is at 1σ around the corrected values). The *direct* MF at $z \sim 4$ (thick histogram) is in good agreement with the uncorrected MF (see text). For masses $> 10^{9.5} M_{\odot}$, the uncorrected $z < 7$ MFs are in rough agreement with the determinations of Stark et al. (2009) and of McLure et al. (2009) at $z \sim 6$ and $\mathcal{M} > 10^{10} M_{\odot}$. The thick dashed curve in each panel represents the *analytic* MFs derived from an idealized $\mathcal{M} - M_{UV,1500}$ relation (see text §4). These MFs have low-mass slopes $\alpha_M \sim -1.4 - -1.6$, slightly flatter than the UV LFs ($\alpha = -1.7 - -2.0$: Bouwens et al. 2010). In turn, the assumed symmetric scatter of 0.5 dex flattens their slopes at the high-mass end. The $z \sim 4$ *analytical* MF is repeated in the other panels for comparison (thin dashed curve). The dotted and thin solid lines show the simulated MFs from Choi & Nagamine (2010) and Finlator et al. (in preparation). Our new results are corrected for incompleteness, yet the difference between our results and the simulations is already substantial by $\mathcal{M} = 10^9 M_{\odot}$. The source of the disagreement is unclear.

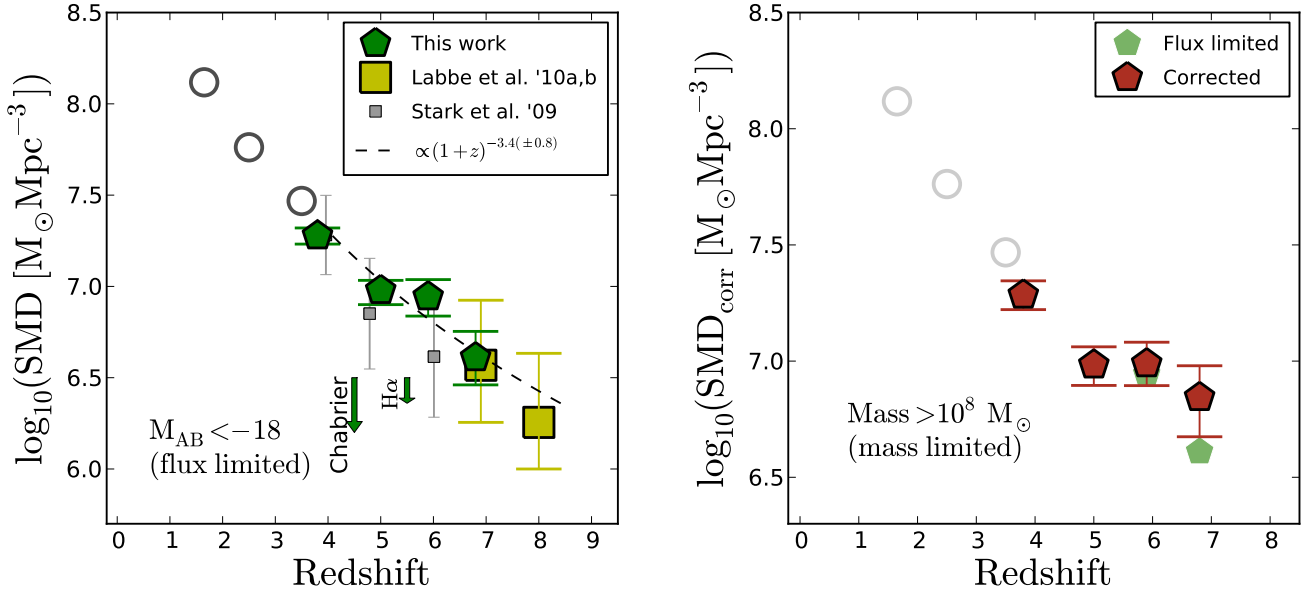


FIG. 4.— (*left*) Stellar Mass Density as a function of redshift for sources brighter than $M_{UV,1500,AB} = -18$. These SMD values are derived by integrating the uncorrected *bootstrap* MFs in Figure 3 to the faint luminosity limit $M_{UV,1500} = -18$ at $z = 4, 5, 6,$ and 7 . For comparison, we show the SMD determinations from Stark et al. (2009) corrected from their original $M_{UV,1500} = -20$ limit to our $M_{UV,1500} = -18$ limit (see text). The low-redshift open circles were derived by integrating the Marchesini et al. (2009) MFs between $8.3 < \log_{10}(\mathcal{M}/M_{\odot}) < 13$ and multiplying by 1.6 to match the Salpeter IMF. A constant SFH and $0.2Z_{\odot}$ metallicity was assumed to derive the masses at $z \gtrsim 4$. The effect of a possible 20% correction due to contamination by $H\alpha$ is shown, as is the effect of using a different IMF. The integrated mass growth we derive with cosmic time is well fit by $\log_{10}(\text{SMD}) \propto (1+z)^{-3.4 \pm 0.8}$. (*right*) As for the left panel but now to a fixed mass limit $> 10^8 M_{\odot}$. The SMD to a fixed mass limit is compared to the flux limited values from the left panel. The differences are relatively small (see text). However, the importance of being able to utilize the completeness-corrected MFs will increase as improved, deeper data becomes available and we can push to lower mass limits.

TABLE 1
SUMMARY OF RESULTS.

	$\langle z \rangle = 3.8$	$\langle z \rangle = 5.0$	$\langle z \rangle = 5.9$	$\langle z \rangle = 6.8$	$\langle z \rangle = 8.0$
COMPLETENESS CORRECTED MASS FUNCTIONS					
$\log_{10}(\mathcal{M}/M_{\odot})$	$\log_{10}(dN/d\log_{10}(\mathcal{M}/M_{\odot})/Mpc^3)$				
[7.5 - 8.0]	$-1.90^{(+.11)}_{(-.12)}$	$-2.21^{(+.18)}_{(-.20)}$	$-2.09^{(+.23)}_{(-.24)}$	$-2.15^{(+.41)}_{(-.39)}$...
[8.0 - 8.5]	$-1.96^{(+.12)}_{(-.12)}$	$-2.27^{(+.18)}_{(-.20)}$	$-2.16^{(+.23)}_{(-.23)}$	$-2.23^{(+.37)}_{(-.38)}$...
[8.5 - 9.0]	$-2.30^{(+.10)}_{(-.11)}$	$-2.60^{(+.15)}_{(-.19)}$	$-2.55^{(+.20)}_{(-.21)}$	$-2.70^{(+.34)}_{(-.36)}$...
[9.0 - 9.5]	$-2.53^{(+.10)}_{(-.11)}$	$-2.84^{(+.17)}_{(-.17)}$	$-2.81^{(+.19)}_{(-.22)}$	$-3.01^{(+.34)}_{(-.34)}$...
[9.5 - 10.0]	$-3.14^{(+.12)}_{(-.13)}$	$-3.46^{(+.17)}_{(-.21)}$	$-3.52^{(+.21)}_{(-.23)}$	$-3.80^{(+.36)}_{(-.37)}$...
[10.0 - 10.5]	$-3.80^{(+.20)}_{(-.23)}$	$-4.12^{(+.22)}_{(-.27)}$	$-4.22^{(+.28)}_{(-.31)}$	$-4.53^{(+.39)}_{(-.61)}$...
[10.5 - 11.0]	$-4.43^{(+.26)}_{(-.46)}$	$-4.81^{(+.33)}_{(-.45)}$	$-4.97^{(+.38)}_{(-.70)}$
SMD ($\mathcal{M} > 10^8 M_{\odot}$) [$10^6 M_{\odot}$]	$19.27^{(+2.88)}_{(-2.62)}$	$9.64^{(+1.88)}_{(-1.78)}$	$9.76^{(+2.30)}_{(-1.91)}$	$6.98^{(+2.57)}_{(-2.26)}$...
SMD ($M_{1500} < -18$) [$10^6 M_{\odot}$]	$18.96^{(+1.94)}_{(-1.90)}$	$9.52^{(+1.27)}_{(-1.58)}$	$8.79^{(+2.11)}_{(-1.91)}$	$4.08^{(+1.59)}_{(-1.19)}$	$1.8^{(+0.7)}_{(-1.0)}$
Best Fit	$\log_{10}(\text{SMD}(z)/[M_{\odot} Mpc^{-3}]) = 7.00^{(+0.04)}_{(-0.05)} - 3.35^{(+0.82)}_{(-0.94)} \times \log_{10}(\frac{1+z}{6})$				

$M_{1500} = -18$ limit by adding 0.18, 0.22, and 0.32 dex at $z \sim 4, 5,$ and 6 respectively. We derive an integrated mass growth across cosmic time that is well fit by the function $\log_{10}(\text{SMD}) \propto (1+z)^{-3.4 \pm 0.8}$. The effect of a different IMF and of a potential contamination by 20% $H\alpha$ at $z \sim 5 - 6$ is also shown on Figure 4.

A major result of this paper is the derivation of MFs corrected for incompleteness at low masses. To utilize the (more representative and accurate) corrected MFs in deriving the SMD of the universe at high redshift we need to integrate to a fixed mass limit. We choose $\mathcal{M} > 10^8 M_{\odot}$ to extend to the limit of our corrected data. The right panel of Figure 4 shows these results, and compares them with the estimates to a fixed luminosity limit (see also Table 1).

The differences are relatively small, less than we expected given the size of the corrections. A number of effects impact the comparison. For the flux-limited ($M_{AB} < -18$) sample, we include relatively bright sources that have masses $> 10^8 M_{\odot}$. In the mass-limited case, we remove those galaxies, and instead include faint sources with large masses. Depending on the limits adopted and the shape of the LF, this effect is more or less important. At $z \sim 7$, the fainter L^* and the steep faint end slope make the difference between what is removed and what is added larger. For the brighter L^* at lower redshifts, however, the difference is almost null.

Nonetheless, the derivation of mass-limited SMDs that appropriately include corrections at low masses is pre-

ferred and will become increasingly important as we push our measurements of the MF to lower limits.

6. KEY RESULTS

We derive stellar masses from SED fits to HST+Spitzer data for over 400 $z \sim 4 - 7$ galaxies. We determine the \mathcal{M} - L_{UV} relation and find it to be steep ($\log(\mathcal{M}) \propto 1.7(\pm 0.2)\log(L_{UV})$) with large intrinsic scatter; the sample variance is ~ 0.5 dex at the bright end. We derive mass functions by combining the \mathcal{M}/L results with published deep UV luminosity functions at $z \sim 4 - 7$, and correct them for incompleteness. The corrected mass functions are steeper ($\alpha \sim -1.4$ to -1.6) than found previously, but still far less steep than those from recent hydrodynamical simulations. The integrated stellar mass density of the universe is derived at $z \sim 4, 5, 6,$ and 7 to $\mathcal{M} \sim 10^8 M_{\odot}$.

We acknowledge insightful discussions with Kristian Finlator, Casey Papovich, Daniel Schaerer, and Daniel Stark. We thank Ken Nagamine, Junhwan Choi and Kristian Finlator for access to their simulations. We acknowledge support from HST-GO10937, HST-GO11563, HST-GO11144, and a Fulbright-CONICYT scholarship (V.G.). I.L. is supported by NASA through a Hubble Fellowship grant #51232.01-A awarded by the Space Telescope Science Institute.

REFERENCES

- Bouwens, R. J., Illingworth, G. D., Franx, M., & Ford, H. 2007, *ApJ*, 670, 928
- Bouwens, R. J., et al. 2010, *ApJ*, submitted, arXiv:1006.4360
- Bruzual, G., & Charlot, S. 2003, *MNRAS*, 344, 1000
- Choi, J., & Nagamine, K. 2010, *MNRAS*, 1042
- de Santis, C., Grazian, A., Fontana, A., & Santini, P. 2007, *New Astronomy*, 12, 271
- Finlator, K., Davé, R., & Oppenheimer, B. D. 2007, *MNRAS*, 376, 1861
- Finlator, K., Oppenheimer, B. D., & Davé, R. 2010, *ArXiv e-prints*
- Giavalisco, M., et al. 2004, *ApJ*, 600, L93
- González, V., Labbé, I., Bouwens, R. J., Illingworth, G., Franx, M., Kriek, M., & Brammer, G. B. 2010, *ApJ*, 713, 115
- Kriek, M., van Dokkum, P. G., Labbé, I., Franx, M., Illingworth, G. D., Marchesini, D., & Quadri, R. F. 2009, *ApJ*, 700, 221
- Labbé, I., Bouwens, R., Illingworth, G. D., & Franx, M. 2006, *ApJ*, 649, L67
- Labbé, I., et al. 2010a, *ApJ*, 716, L103
- . 2010b, *ApJ*, 708, L26
- Madau, P., Pozzetti, L., & Dickinson, M. 1998, *ApJ*, 498, 106
- Marchesini, D., van Dokkum, P. G., Förster Schreiber, N. M., Franx, M., Labbé, I., & Wuyts, S. 2009, *ApJ*, 701, 1765
- McLure, R. J., Cirasuolo, M., Dunlop, J. S., Foucaud, S., & Almaini, O. 2009, *MNRAS*, 395, 2196
- Oke, J. B., & Gunn, J. E. 1983, *ApJ*, 266, 713
- Papovich, C., Dickinson, M., & Ferguson, H. C. 2001, *ApJ*, 559, 620
- Papovich, C., Finkelstein, S. L., Ferguson, H. C., Lotz, J. M., & Giavalisco, M. 2010, arXiv:1007.4554
- Salpeter, E. E. 1955, *ApJ*, 121, 161
- Stark, D. P., Ellis, R. S., Bunker, A., Bundy, K., Targett, T., Benson, A., & Lacy, M. 2009, *ApJ*, 697, 1493
- Windhorst, R. A., et al. 2010, arXiv:1005.2776
- Wuyts, S., et al. 2007, *ApJ*, 655, 51
- Yan, H., et al. 2005, *ApJ*, 634, 109